Geoscientific
Model Development

Open Access

EGU

Supplement of

Cohesive and mixed sediment in the Regional Ocean Modeling System (ROMS v3.6) implemented in the Coupled Ocean–Atmosphere–Wave–Sediment Transport Modeling System (COAWST r1234)

C. R. Sherwood et al.

Correspondence to: Christopher R. Sherwood (csherwood@usgs.gov)

1 Introduction

This Supplement provides additional details and formulae describing the cohesive- and mixed-sediment algorithms, and a guide to variables and keywords used to control model options. Some of the material from the main paper is repeated here to aid readability.

This supplement describes parts of the COAWST implementation of ROMS version 3.6 (COAWST Subversion revision 1234, distributed by the U.S. Geological Survey. Contact jcwarner@usg.gov). The source code for ROMS is distributed among several directories. Most of the code dealing with sediment is in the directory `COAWST\ROMS\Nonlinear\Sediment`. This includes the non-cohesive routines developed as part of the Community Sediment-Transport Modeling System (CSTMS) and described by Warner et al., 2010, and the new cohesive and mixed-bed routines described in the main paper. Two example applications are provided in the `COAWST\Projects\Sed_floc_toy` and `COAWST\Projects\Sedbed_toy` folders.

Many ROMS options are specified using keywords parsed by the C Pre-processor (CPP) routine prior to model program compilation. These keywords are selected by users in application-dependent include (or header; `.h`) files. In this supplement, keywords are denoted in UPPER_CASE, and file names are denoted with `monospace` font. Table S1 provides a list of the notation used in the equations and Table S2 lists the associated ROMS variable names as they appear in input or output files. Table S3 lists ROMS variables required in the input files, and Table S4 lists ROMS variables used to track seabed properties.

2 Model Algorithms

The sediment algorithms implemented as part of ROMS follow the schematic presented in Figure S1. The water-column dynamics are coupled with the sediment dynamics at each model time step. Inside the sediment module, the main routine (`sediment.F`) controls the execution of the user-selected sediment behavior options. Separate routines calculate bottom-boundary layer hydrodynamics (wave-current interaction, hydrodynamic roughness, and bed shear stresses), bedload transport, suspended-sediment

settling, flocculation and disaggregation, erosion and deposition, and changes in bed sediment properties.

The new contributions that simulate cohesive and mixed sediment include a floc model for particle flocculation and disaggregation in the water column, and several procedures for cohesive and mixed behavior in the seabed.

2.1 Floc Model

The floc model FLOCMOD of Verney et al. (2011) is implemented in the ROMS routine `sed_flocs.F`. FLOCMOD treats a finite number (NCS, Number of Cohesive Sediment classes) of size classes with representative floc diameters D_f (m). The model assumes that floc densities ρ_f (kg/m^3) decrease with size, and are related to the primary disaggregated particle diameter D_p (m) and density ρ_s (kg/m^3) through a fractal dimension n_f (dimensionless; Kranenburg, 1994) according to

$$\rho_f = \rho_w + \left(\rho_s - \rho_w\right)\left(\frac{D_f}{D_p}\right)^{n_f - 3} \qquad \text{(S 1)}$$

where ρ_w (kg/m^3) is the density of the interstitial water in the flocs (Table 1). The mass m (kg) of an individual floc is therefore

$$m = \rho_s \frac{\pi}{6} D_p^3 \left(\frac{D_f}{D_p}\right)^{n_f} \qquad \text{(S 2)}$$

The fractal dimension for natural flocs is typically close to 2.1 (Tambo and Watanabe, 1979; Kranenburg, 1994). Floc densities increase as n_f increases, and at $n_f = 3$, the flocs are solid particles with $\rho_f = \rho_s$. When the floc model is used in ROMS (CPP keyword SED_FLOCS is defined), all cohesive sediment classes are treated as flocs and the processes of aggregation and disaggregation can act to shift mass of suspended sediment from one class to another.

Users are responsible for providing cohesive sediment parameters in the input file `sediment.in` that are consistent with Equation (S 1). An example is provided in `COAWST\Projects\Sed_floc_toy\sediment_sed_floc_toy.in`. Verney et al. (2011) report that at least eight floc classes were required to reproduce the results of their lab experiment.

FLOCMOD simulates two-particle interactions that result in aggregation after collisions caused by either shear or differential settling, and disaggregation caused by turbulence

2

shear and/or collisions. The rate of change in the number concentration $N(k)$ (m^{-3}) of particles in the kth floc class is controlled by a coupled set of linear equations

$$\frac{dN(k)}{dt} = G_a(k) + G_{bs}(k) + G_{bc}(k) - L_a(k) - L_{bs}(k) - L_{bc}(k) \qquad \text{(S 3)}$$

where k is the particle class, and G (m^{-3} s^{-1}) and L (m^{-3} s^{-1}) terms represent gain and loss of mass by the three processes denoted by subscripts: a (aggregation), bs (breakup caused by shear), and bc (breakup caused by collisions). Equations (S 3) are integrated explicitly using adjustable time steps that may be as long as the baroclinic model time step, but are decreased automatically when necessary to ensure that particle number concentrations remain positive. Particle number concentrations $N(k)$ are related to suspended mass concentrations $C_m(k)$ (kg/m^3) via the mass of the individual flocs m as

$$N(k) = C_m(k) / m(k) \qquad \text{(S 4)}$$

The aggregation terms in Equations (S 3) include gain in class k caused by collisions between classes i and j

$$G_a(k) = \tfrac{1}{2} \sum_{i+j=k} \alpha_{ij} A(i,j) N_i N_j \qquad \text{(S 5)}$$

and loss from class k by accretion into class i

$$L_a(k) = \sum_{1}^{N} \alpha_{ij} A(i,k) N_i N_k \qquad \text{(S 6)}$$

where α is the collision efficiency and $A(i,j)$ is the probability function for two-particle shear-induced collisions between classes i and j. In general, the collision efficiency depends on environmental factors (temperature, salinity) and the nature (shape, mineral composition, organic-matter content, etc.) of the two particle classes, but in our implementation, a universal collision efficiency is used. The probability of shear-induced collision depends on the particle diameters D_f (m) and the shear rate $G = \sqrt{\varepsilon / \nu}$ (s^{-1}), where ε (m^2/s^3) is the turbulence dissipation rate and ν (m^2/s) is the kinematic viscosity of the fluid:

$$A(i,j) = \tfrac{1}{6} G (D_i + D_j)^3 \qquad \text{(S 7)}$$

FLOCMOD includes terms for collisions caused by differential settling but, because shear-induced collisions are much more effective in turbulent environments, we have not exercised that part of the code.

3

The turbulence dissipation rate ε is computed from the turbulence submodel in ROMS. For example, when the generic length scale equation (Umlauf and Burchard, 2002; Warner et al., 2005) is used

$$\varepsilon = \left(c_\mu^0\right)^{3+gls\_p/gls\_n} tke^{3/2+gls\_m/gls\_n} gls^{-1/gls\_n} \tag{S 8}$$

where c_μ^0 is the stability coefficient, *tke* is turbulent kinetic energy, *gls* is the second, generic parameter in the turbulence submodel, and *gls_p*, *gls_n*, and *gls_m* are coefficients that define the submodel. These coefficients are provided as user input, usually as one of four specific combinations that define one of three classic turbulence closures or a fourth generic closure of Umlauf and Burchard (2002; see Table 1 in Warner et al., 2005).

The shear-breakup terms in Equations (S 3) for gain or loss in class *k* due to fragmentation in larger classes *i* are

$$G_{bs}(k) = \sum_{i=k+1}^{n} \text{FDBS}_{ki} B_i N_i \tag{S 9}$$

and

$$L_{bs}(k) = B_k N_k \tag{S 10}$$

where the fragmentation rate B_i for class *i* is

$$B_i = \beta_i G^{3/2} D_{f,i} \left(\frac{D_{f,i} - D_p}{D_p} \right)^{3-n_f} \tag{S 11}$$

where β_i is a fragmentation rate that depends on the yield strength of the flocs. FDBS is a function that determines how much of the mass appears in class *k* when a particle in class *i* breaks up due to shear. The exponents in Equation (S 11) follow from Winterwerp's (2002) assumption that equilibrium floc size is related to the Komogorov microscale. Three distribution functions are implemented to characterize floc breakup in FLOCMOD (Verney et al., 2011): binary distribution (flocs break into two equal sizes, each with half of the mass); ternary distribution (flocs break into three parts, one with half of the mass, and two with a quarter of the mass); and erosion (flocs break into one large fragment and *n* smaller fragments, where the mass of the large fragment is reduced by *n* times the mass of the smaller fragments; Hill, 1996). The relative contribution of each of these breakup distribution functions is controlled by model parameters discussed below.

4

Collision-induced breakup terms in Equations (S 3) are defined as proposed by McAnally and Mehta (2001) as

$$G_{bc}(k) = \sum_{ij} \text{FDBC}_{ij} A(i, j) N_i N_j \tag{S 12}$$

$$L_{bc}(k) = \sum_{i=1}^{n} \text{FDBC}_{ik} A(i, k) N_i N_k \tag{S 13}$$

where FDBC is the function that determines the distribution of fragments after a collision. It depends on the collision-induced shear stress τ^{coll} (Pa) and the strength τ^y (Pa) of the particles. The collision-induced shear stress experienced by particle in class i during a collision with a particle in class j is

$$\tau_{ij,i}^{coll} = \frac{8\left(G(D_{f,i} + D_{f,j})/2\right)^2 m_i m_j}{\pi F_p D_i^2 (D_{f,i} + D_{f,j})(m_i + m_j)} \tag{S 14}$$

where F_p is a relative depth of interparticle penetration estimated as $F_p = 0.1$ (Krone, 1963; McAnally, 1999; McAnally and Mehta, 2001). Particle strength depends on floc density ρ_i :

$$\tau_i^y = F_y \left(\frac{\rho_w - \rho_{f,i}}{\rho_w}\right)^{2/(3-n_f)} \tag{S 15}$$

where F_y (Pa) is the floc yield strength, taken as $10^{-10} N$ (Winterwerp and van Kesteren, 2004). If the collision-induced shear stress exceeds the particle strength of only one of the two colliding particles, the weaker particle (class j) breaks into two fragments: a larger one with mass $13/16 m_j$, and a smaller one with mass $3/16 m_j$ that binds with the stronger particle. If the collision-induced stress is greater than the particle strength of both classes, then each particle breaks into two parts, producing particles with masses $13/16 m_i$, $3/16 m_i$, $13/16 m_j$, and $3/16 m_j$. The smaller fragments bind to form a particle with mass $3/16 m_i + 3/16 m_j$ (McAnally, 1999; McAnally and Mehta, 2001).

Floc model parameters

The floc model introduces several parameters (Table 2), some of which have been evaluated by Verney et al. (2011). These parameters are specified by the user as input to the model in the `sediment.in` file. We have not performed an extensive sensitivity analysis for these parameters, but others indicate that the equilibrium floc size depends on the ratio of aggregation to breakup parameters, and the rate of floc formation and destruction depends on their magnitudes (Winterwerp, 1999; 2002).

The diameter, settling velocity, density, critical stress for erosion, and critical stress for deposition are also specified as inputs for each sediment class (Table 3). We have assumed, for the cases presented here, a fractal relationship between floc diameter and floc density (Equation (S 1); Kranenburg, 1994) and a Stokes settling velocity w (m/s):

$$w_i = \frac{(\rho_i - \rho_w)gD_{f,i}^2}{18\mu} \tag{S 16}$$

where $\mu \approx 0.001$ Pa·s is the dynamic viscosity of the fluid. Alternative relationships between diameter and settling velocity exist, such as modified Stokes formula (e.g., Winterwerp, 2002; Winterwerp et al., 2007; Droppo et al., 2005; Khelifa and Hill, 2006). The relationship between diameter and floc density described in Equation (S 1) cannot be changed, however, without significant modifications to portions of the model code that ensure mass conservation as sediment changes classes during aggregation and disaggregation.

Fluxes into the bed – Critical shear stress for deposition

The settling flux of flocs (and all other size classes) into the bed (deposition) over a time step is calculated as $w_i\rho_iC_{v,i}\Delta t$, where w_i, ρ_i, and $C_{v,}$ are the settling velocity, floc (or particle) density, and volume concentration for the ith size class in the bottom-most water-column layer, respectively, and Δt is the model time step. ROMS calculates the settling flux in `sed_settling.F`. The concept of a critical stress for deposition τ_d (Pa) (Krone, 1962; Whitehouse et al., 2000; Mehta, 2014) has been implemented as an option; if selected, deposition is zero when the bottom stress τ_b exceeds τ_d, and increases linearly as τ_b decreases below τ_d (Whitehouse et al., 2000), as follows.

$$\begin{aligned}(1-\tau_b/\tau_{d,i})w_i\rho_iC_{v,i}\Delta t \quad \text{for} \quad \tau_b < \tau_{d,i} \\ 0 \quad \text{for} \quad \tau_b \geq \tau_{d,i}\end{aligned} \tag{S 17}$$

We call this linear depositional flux, and it is invoked with CPP option SED_TAU_CD_LIN.

A simpler alternative is to assume a full settling flux when $\tau_b < \tau_d$, which we call constant depositional flux:

$$\begin{aligned}w_i\rho_iC_{v,i}\Delta t \quad \text{for} \quad \tau_b < \tau_{d,i} \\ 0 \quad \text{for} \quad \tau_b \geq \tau_{d,i}\end{aligned} \tag{S 18}$$

which is invoked with SED_TAU_CD_CONST. The calculations are performed in `sed_fluxes.F`. The critical stress for deposition for each size class $\tau_{d,i}$ for both cohesive

and non-cohesive classes must be specified as input; large values effectively nullify the calculation, particularly when using the constant depositional flux (Equation (S 18)). Earlier versions of the CSTMS included these input variables as placeholders but did not use them. There is not a consensus on specifying τ_d. According to Whitehouse et al. (2000), τ_d is typically about one-half the magnitude of the critical shear stress for erosion τ_c, but is unrelated to that value. Mehta (2014, Equation 9.83) suggests

$$\tau_d = \tau_{dp} \left(D_{f,i} / D_p \right)^{\xi}$$ (S 19)

where τ_{dp} is τ_d for the smallest particle diameter D_p and ξ is an exponent that depends on sediment properties. Mehta (2014) lists values of $\tau_{dp} = 0.03$ Pa and $\xi = 0.5$ for kaolinite with $D_p = 1 \ \mu$m, citing Letter (2009) and Letter and Mehta (2011). The effect of either Equation (S 17) or Equation (S 18) when $\tau_b \geq \tau_d$ is to prevent deposition and keep sediment in suspension in the bottom layer. This allows the material to be transported as suspended sediment and, for flocs, allows aggregation and disaggregation processes to continue.

Changes in floc size distribution within the bed

It seems reasonable to expect changes in the size-class distribution of flocs once they have been incorporated into the seabed, in contrast to non-cohesive particles that retain their properties during cycles of erosion and deposition. For example, it seems unlikely that large, low-density flocs can be buried and later resuspended intact, and limited published observations suggest that material deposited as flocs can be eroded as denser, more angular aggregates (Stone et al., 2008). However, we find little guidance for constraining this process. We therefore have implemented a simple formulation that allows the user to stipulate an equilibrium cohesive size-class distribution and an associated relaxation time scale, as described below. The user-specified equilibrium distribution controls the size classes in the bed that are resuspended when cohesive bed material is eroded.

The calculations to specify changes to floc distribution in the bed are made in `sed_bed_cohesive.F` when the CPP option SED_DEFLOC is invoked. The equilibrium fractional distribution f_{ceq} of the cohesive size classes in the bed is specified as input. In bed layers (except the top, active layer), the equilibrium mass distribution is calculated as

$$m_{eq,i} = f_{ceq,i} m_{tot}$$ (S 20)

where m_{tot} is the sum of the mass in all of the cohesive classes in that bed layer:

$$m_{tot} = \sum_{i=1}^{NCS} m_i \qquad \text{(S 21)}$$

where NCS is the number of cohesive classes. The floc distribution in a layer is nudged toward the equilibrium distribution according to

$$m_i^{new} = m_i^{old} + c(m_{eq,i} - m_i^{old}) \qquad \text{(S 22)}$$

where the nudging coefficient c is determined by the model time step Δt and the user-specified time scale t_{eq} as

$$c = \min(1, \Delta t / t_{eq}) \qquad \text{(S 23)}$$

This formulation conserves mass, but does not achieve full equilibrium unless $t_{eq} \leq \Delta t$. Test cases presented in Section 3 of the main paper demonstrate the effect of this process and the associated time scale on floc distributions both in the bed and in the water column.

2.2 Properties of sediment, seafloor, and seabed.

The model accounts for two distinct types of sediment: non-cohesive sediment (e.g., sand) and cohesive sediment (e.g., mud). The general framework is unchanged from Warner et al. (2008), except that the expanded model requires additional variables to allow for both cohesive and non-cohesive types. The number of sediment classes of each type is, at present, limited to twenty-two by input/output formatting protocols. The total number of sediment classes, NSED, equals the sum of the number of non-cohesive (NNS) and cohesive (NCS) classes. At least one class of one type is required for sediment-transport modeling. Classes may be used to represent sediment with a range of properties that are specified by the user, and remain constant throughout the model calculations. Sediment properties are stored in two one-dimensional arrays (one for non-cohesive sediment and one for cohesive sediment) and include particle diameter, sediment density, settling velocity, critical shear stress for erosion, critical shear stress for deposition (this value is presently ignored for non-cohesive sediment), erosion-rate coefficient, and porosity (Table 3).

Seafloor properties describe the condition of the sediment surface and are stored in arrays with two spatial dimensions that correspond to the horizontal model domain (Warner et al., 2008). Seafloor properties (Table S4) include representative values (geometric means) of sediment in the top layer, including grain size, critical shear stress for erosion, settling velocity, and density; and properties of the sediment surface, such as

8

ripple height, ripple wavelength, and bottom roughness. These properties may be specified as input, or calculated in the model. The arrays are also used to store additional parameters if cohesive or mixed sediment calculations are being performed, as discussed below.

Seabed properties (i.e. stratigraphy) are stored with three spatial dimensions representing horizontal location and layer in the bed. As with other model dimensions, the number of layers used to represent seabed properties (NBED) is specified in user input files and remains constant throughout the model run. Each sediment bed layer stores information, including the mass of each sediment class, porosity, and age. The layer thickness, which is derived from mass and sediment density for each class and porosity, is stored for convenience, as is the depth to the bottom of each layer. To account for consolidation and swelling, the framework used in Warner et al. (2008) with modificatons discussed in the next section, has been augmented to store additional information for bulk critical shear stress τ_{cb} in each bed layer if cohesive sediment formulations are enabled with CPP keywords COHESIVE_BED or MIXED_BED.

2.3 Stratigraphy

Representation of seabed properties, i.e. the stratigraphy, has been modified slightly from the framework presented in Warner et al. (2008). Here we summarize the overall scheme for the sediment bed layers, emphasizing the modifications to the model beyond the Warner et al. (2008) framework.

Stratigraphy serves two functions in the model as conditions change and sediment is added or removed from the bed: (1) to represent the mixture of sediment available at the sediment-water interface for use in bedload transport, sediment resuspension, and roughness calculations; and (2) to record the depositional history of sediment. Algorithms for tracking and recording stratigraphy must conserve sediment mass and must accurately record and preserve age, porosity, and other bulk properties that apply to each layer. Ideally, a layer could be produced for each time step in which deposition occurs, and a layer could be removed when cumulative erosion exceeds layer thickness. In practice, the design of many models (including ROMS) adds an additional constraint: the number of layers (NBED) used to record stratigraphy is declared at the beginning of the model run and cannot change. Thus, when deposition creates a new layer, or when erosion removes a layer, layers must be merged and split so that the total number of layers remains equal to NBED. Where and when this is done determines the fidelity and utility of the modeled stratigraphic record. Some models have used a constant layer thickness (Harris and

Wiberg, 2001); others (for example, ECOMSED) define layers as isochrons deposited within a fixed time interval (HydroQual, Inc., 2004). Our approach is most similar to that described by Le Hir et al. (2011) in that we allow mixing of deposited material into the top layer, and require a minimum thickness of newly formed layers, merging the bottom layers when a new layer is formed.

A key component of the bed model is the active layer (Hirano, 1971), which is the thin (usually mm-scale), top-most layer of the seabed that participates in exchanges of sediment with the overlying water. During each model time step, deposition and erosion may contribute or remove mass from the active layer. One disadvantage of this approach is that any stratigraphy in the active layer is lost by instantaneous mixing (Merkel and Klopmann, 2012), but this is consistent with the original concept of Hirano (1971) and the need to represent the spatially averaged surface sediment properties in a grid cell that represents a heterogeneous seabed. For non-cohesive sediment, Warner et al. (2008) set the active-layer thickness $\Delta z_a = \max[k_1(\tau_{sf} - \langle \tau_c \rangle), 0] + k_2 \langle D \rangle$, where τ_{sf} (Pa) is the skin friction component of the wave-current combined bottom shear stress, and $\langle \tau_c \rangle$ (Pa) is the critical shear stress for erosion of the particles in the active layer, $\langle D \rangle$ (m) is the representative diameter of particles in the active layer, and k_1 and k_2 are dimensional empirical coefficients with values of 0.007 and 6, respectively (Harris and Wiberg, 1997). The brackets indicate that $\langle \tau_c \rangle$ and $\langle D \rangle$ are determined as the fraction-weighted geometric mean from contents of the active layer at the end of the previous time step. When COHESIVE_BED is enabled, the active layer thickness is defined as the depth where the bulk critical shear stress of the sediment bed exceeds the bottom shear stress, so sediment is available for resuspension in the layer $z < z_\rho$ where $\tau_b > \tau_{cb}(z_\rho)$. When MIXED_BED is enabled, the active layer thickness is calculated using both methods, and the greater of the two values is used.

The bed model conserves mass and maintains a constant number of layers (NBED), even during erosional or depositional cycles. The thickness of the top layer at the start of each time step is equal to the active-layer thickness Δz_a determined during the previous step. These are unchanged from Warner et al., 2008. However, improved fidelity of the stratigraphic record is obtained with a revised sequence of layer calculations that occur when COHESIVE_BED, MIXED_BED, or (for non-cohesive simulations) SED_BED2 is enabled, as follows. (1) Mass associated with deposition or erosion of each class is added or subtracted to the top layer. Erosion in each class is limited to the mass of that class available in the active layer. (2) The new Δz_a is calculated, based on stresses from the current time step and sediment properties from the previous time step. (3) If the top

layer is thinner than Δz_a, material from sequentially deeper layers is merged to form a top layer with thickness Δz_a. If, instead, the top layer is thicker than Δz_a, excess sediment is placed in the second layer. The user-specified value $\Delta z_{nl\,max}$ is used to constrain the thickness of the second layer during deposition, so that continued deposition produces multiple layers, none of which are thicker than $\Delta z_{nl\,max}$. (4) If deposition requires formation of one or more layers (beneath the top layer), the bottom-most layers are merged to maintain NBED layers. If, on the other hand, layers have been merged, one or more thin layers (with thickness $\Delta z_{nl\,max}$; see below) are split from the bottom layer to maintain NBED layers. The new layers are assigned properties (grain size, porosity, etc.) identical to those of the original bottom layer. Note that the original formulation in Warner et al. (2008) split the bottom layer into equal halves to form an additional layer. (5) The final step in the bed model calculates age and porosity of each layer as mass-weighted arithmetic means. Representative seafloor properties associated with the sediment in the top layer, including $\langle D \rangle$, $\langle \tau_c \rangle$, $\langle w_s \rangle$, and $\langle \rho_s \rangle$ are calculated as geometrical means, weighted by the fractional amount of each sediment class in the layer.

The revised bed model gives the user latitude to control the resolution of the bed model through the choice of values for $\Delta z_{nl\,max}$ and NBED, and avoids the mixing described by Merkel and Klopmann (2012). The main differences from previous versions of the model (Warner et al., 2008) are the treatments of the second layer (immediately below the active layer) and the bottom layer. During deposition, the new algorithm prevents the second layer from becoming thicker than $\Delta z_{nl\,max}$, which results in thinner layers that can record changes in sediment composition inherited from the active layer as materials settle. During erosion, the new algorithm splits off only a small portion of the bottom layer to create a new layer with thickness $\Delta z_{nl\,max}$ unless the bottom layer is thinner than $\Delta z_{nl\,max}$, in which case the bottom layer is split. This limits the influence of the initial stratigraphy specified for the bottom layer and confines blurring of the stratigraphic record the bottommost layers. Our tests indicate the new approach provides a more informative record of stratigraphic changes, and Moriarty et al. (2017) used a similar approach to bed stratigraphy to preserve spatial gradients in sediment biogeochemistry.

2.4 Bulk Critical Shear Stress for Cohesive Sediment

When the cohesive bed model is invoked (CPP keyword COHESIVE_BED), the erodibility depends on the bulk critical shear stress τ_{cb} (Pa), which is a property of the bed layer, not individual sediment classes. The bulk critical shear stress generally increases

with depth in the bed, and changes with erosion, deposition, swelling, and consolidation. The cohesive bed model tracks these changes by updating profiles of τ_{cb} at each grid point and time step.

There is no generally accepted physically based model for determining τ_{cb} from bed properties such as particle size, mineralogy, and porosity. We adopted Sanford's (2008) heuristic approach based on the concept that the bulk critical shear stress profile tends toward an equilibrium profile $\tau_{cb\,eq}(z)$ (Figure 1 in main paper). This method tracks only τ_{cb} instead of directly modeling consolidation, swelling, and other physical process responsible for altering bed critical stresses. The $\tau_{cb\,eq}$ profile depends on depth in the seabed and must be determined a priori. Erosion-chamber measurements have been used to define this equilibrium bulk shear stress profile $\tau_{cb\,eq}$ (Sanford, 2008; Rinehimer et al., 2008; Dickhudt et al., 2009; Dickhudt et al., 2011; Butman et al., 2014). The equilibrium bulk shear stress profile is defined using two parameters, *offset* and *slope*:

$$\tau_{cb\,eq} = a \exp\left[\left(\ln\left(z_\rho\right) - offset\right) / slope\right] \qquad (S\ 24)$$

where *offset* and *slope* have units of ln(kg/m^2), and $a = 1$ Pa kg^{-1} m^2 is a dummy coefficient that produces the correct units of critical shear stress. The mass depth, z_ρ (kg/m^2) is the cumulative dry mass of sediment overlying a given depth in the bed, so the mass depth at the bottom of each model layer *k* is calculated as

$$z_\rho(k) = \sum_{k=1,NBED} \sum_{i=1,NSED} f_{i,k}\rho_i\Delta z_k \qquad (S\ 25)$$

Equation (S 24) can be related to the power-law fits to erosion-chamber measurements presented by Dickhudt (2008) and Rinehimer et al. (2008), which take the form

$$\tau_{ec} = a' m_{ec}{}^b \qquad (S\ 26)$$

where m_{ec} is the cumulative mass eroded at an applied erosion-chamber shear stress τ_{ec} and *a'* and *b* are dimensional coefficients, with $slope = 1/b$ and $offset = -slope\ln(a')$. In the model, the equilibrium stress profile is further bounded with

$$\tau_{cb\min} \leq \tau_{cb\,eq} \leq \tau_{cb\max} \qquad (S\ 27)$$

where the user-provided minimum and maximum values $\tau_{cb\min}$ and $\tau_{cb\max}$ apply at the sediment water interface and deep in the sediment, respectively. The instantaneous profile is nudged toward the equilibrium profile to represent the effects of consolidation or swelling following perturbations caused by erosion or deposition:

$$\frac{\Delta \tau_{cb}}{\Delta t} = \begin{cases} \dfrac{1}{T_c}\left(\tau_{cb\,eq} - \tau_{cb}\right), & \tau_{cb} < \tau_{cb\,eq} \\[2mm] 0, & \tau_{cb} = \tau_{cb\,eq} \\[2mm] -\dfrac{1}{T_s}\left(\tau_{cb\,eq} - \tau_{cb}\right), & \tau_{cb} > \tau_{cb\,eq} \end{cases} \tag{S 28}$$

where T_c (s) is the time scale for consolidation and T_s (s) is the time scale for swelling. The consolidation time scale is usually chosen to be much shorter ($T_s \sim 10^{-2} T_c$) than the one associated with swelling (Sanford, 2008). New sediment deposited to the surface layer is assigned a bulk critical shear stress that may either be (1) held constant at a low value (Rinehimer et al. 2008), or (2) set at the instantaneous bed shear stress of the flow.

2.5 Mixed Sediment

The mixed-sediment algorithm is intended to ensure reasonable behavior when both cohesive and non-cohesive sediment are present in a model domain. The algorithm depends on the mud fraction in the bed. Beds with low mud content behave according to rules for non-cohesive sediment and erodibility is determined by critical shear stress of the particles present in the active layer. Non-cohesive beds may be winnowed and armored by selective erosion of the finer fraction. In contrast, beds with high mud content behave according to bulk properties that, in the model, are characterized by the bulk critical shear stress for erosion. Mixed beds have intermediate mud content and their critical shear stress in the model is a weighted combination of cohesive and non-cohesive values.

We define a cohesive-behavior parameter P_c (dimensionless) that characterizes the extent to which the bed sediment behaves cohesively. Where $P_c = 0$, there is no cohesive behavior, and the particle shear stress τ_c for each sediment class is used as the effective critical shear stress τ_{ce} for that class. Where $P_c = 1$, the cohesive sediment algorithm is used, and the effective critical shear stress for each class is the greater of τ_{ce} and the bulk critical shear stress τ_{cb}. Between those limits, the effective critical shear stress for each sediment class is

$$\tau_{ce} = \max\left[P_c \tau_{cb} + \left(1 - P_c\right)\tau_c, \quad \tau_c \right] \tag{S 29}$$

The overall proportion of sediment in cohesive classes f_c in the active mixed layer determines the cohesive behavior parameter P_c:

13

$$f_c = \frac{\displaystyle\sum_{i=1,NCS} f_i \rho_i}{\displaystyle\sum_{i=1,NCS} f_i \rho_i + \sum_{i=1,NNS} f_i \rho_i} \tag{S 30}$$

where f_c quantifies the overall mud content in the bed, f_i is the volume fraction, and ρ_i is the sediment grain density of sediment class i. Material behaves non-cohesively ($P_c = 0$). where $f_c \leq f_{nc\,thresh}$. Typical values of $f_{nc\,thresh}$ are ~0.03 – 0.10, indicating that a cohesive sediment content of more than a few percent changes the behavior of the bed (Mitchener and Torfs, 1996; Panagiotopoulos et al., 1997; van Ledden et al., 2004; Jacobs et al., 2011). Completely cohesive behavior occurs when f_c exceeds $f_{c\,thresh}$ which typically has values of ~0.20 – 0.30. Between those limits, P_c changes linearly:

$$P_c = \begin{cases} 0, & f_c \leq f_{nc\,thresh} \\ \min\left[\max\left(\dfrac{f_c - f_{nc\,thresh}}{f_{c\,thresh} - f_{nc\,thresh}}\right),\ 0\right], & f_{nc\,thresh} < f_c < f_{c\,thresh} \\ 1, & f_c \geq f_{c\,thresh} \end{cases} \tag{S 31}$$

This approach allows fine material (e.g., clay) to be easily resuspended when only a small fraction of mud is present in an otherwise sandy bed, and it limits the flux to the amount available in the active mixed layer. It also allows non-cohesive silt or fine sand embedded in an otherwise muddy bed to be resuspended during bulk erosion events, and it provides a simple and smooth transition between these behaviors. The thickness of the active mixed layer is calculated as the thicker of the cohesive and non-cohesive estimates. The behavior is discussed in Section 3 of the main paper and illustrated in Figure 3.

2.6 Bed Mixing

Mixing of bed properties in sediment can be caused by infauna (ingestion, defecation, or motion such as burrowing) or circulation of porewater, and tends to smooth gradients in stratigraphy and move material vertically in sediment. The model assumes that mixing is a vertical diffusive process and neglects non-local mixing processes; see Boudreau (1997) for a more complete discussion of mixing models for sediment. Mixing is described by the diffusion equation

$$\frac{\partial C_v}{\partial t} = \frac{\partial}{\partial z}\left(D_b \frac{\partial C_v}{\partial z}\right) \tag{S 32}$$

where C_v (m^3/m^3) is the volume concentration of a conservative property (e.g., fractional concentration of sediment classes or porosity), D_b is a (bed-depth-dependent)

14

(bio)diffusion coefficient (m^2/s), and z (m) is depth in the bed (zero at the sediment-water interface, positive downward). Zero-flux boundary conditions are imposed at the top and bottom of the sediment bed, and a fully implicit numerical solution is used that is unconditionally stable and conserves bed properties.

The depth-dependent biodiffusion coefficient profile in the model can be specified for each horizontal grid cell. The shape of the profile $D_b(z)$ is specified using five parameters, as follows (Figure S2).

$$D_b = \begin{cases} D_{bs}, & z \leq z_s \\ D_{bs} \exp\left(\dfrac{-z - z_s}{r}\right), & z_s < z \leq z_m \\ D_{bm} - \dfrac{D_{bm}}{z_{zero} - z_m}(z - z_m), & z_m < z \leq z_{zero} \\ \sim 0, & z > z_{zero} \end{cases} \tag{S 33}$$

where

$$r = \frac{-z_m - z_s}{\log\left(D_{bm} / D_{bs}\right)} \tag{S 34}$$

where z_s, z_m, and z_{zero} are depths in the bed (m). D_{bs} represents the biodiffusivity from the surface to depth z_s, and is the value used for the biodiffusion coefficient to depth z_s. Between depths z_s and z_m, the biodiffusion coefficient decreases exponentially from D_{bs} to D_{bm}. Between depths z_m and z_{zero}, biodiffusivity decreases linearly from D_{bm} to a small background value, where it remains below z_{zero}. Uniform, exponential, and linear portions of the profile can be expanded, contracted, or eliminated by manipulating z_s, z_m, and z_{zero}. This method of defining the biodiffusivity profile was chosen for flexibility and has been used to represent sediment mixing on the Palos Verdes shelf, CA (Sherwood et al., 2002), and the Rhone subaqueous delta (Moriarty et al. 2017).

We evaluated the numerical characteristics of the implemented biodiffusion algorithm. The convergence and sensitivity was tested by comparing numerical solutions with known analytical solutions (Fischer et al., 1979) for two cases (not shown): point-source diffusion (Dirac case) and diffusion across a step in concentration (Heaviside case). The solution was accurate to first order with truncation error governed by the time step and square of the layer thickness. For typical time steps used in regional-scale ocean models (~seconds to minutes) and ~mm- to cm-scale bed layer thickness, the numerical

15

solution behaved well. The algorithm conserved mass and also behaved appropriately for non-uniform bed thicknesses and for spatially variable diffusivities.

References

Boudreau, B. P.: Diagenetic Models and Their Implementation, Springer-Verlag, Berlin, 414 pp, 1997.

Butman B., Aretxabaleta, A. L., Dickhudt, P. J., Dalyander, P. S., Sherwood, C. R., Anderson, D. M., Keafer, B. A., and Signell, R. P.: Investigating the importance of sediment resuspension in Alexandrium fundyense cyst population dynamics in the Gulf of Maine, Deep-Sea Res. PT II, 103, 74−95, doi:10.1016/j.dsr2.2013.10.011, 2014.

Dickhudt, P. J.: Controls on erodibility in a partially mixed estuary: York River, Virginia, M. S. Thesis, College of William and Mary, Gloucester Point, VA, 2008.

Dickhudt, P. J., Friedrichs, C. T., Schaffner, L. C., and Sanford, L. P.: Spatial and temporal variation in cohesive sediment erodibility in the York River estuary, eastern USA: A biologically influenced equilibrium modified by seasonal deposition, Mar. Geol., 267, 3−4, 128−140. doi:10.1016/j.margeo.2009.09.009, 2009.

Dickhudt, P. J., Friedrichs, C. T., and Sanford, L. P.: Mud matrix solids fraction and bed erodibility in the York River estuary, USA, and other muddy environments, Cont. Shelf Res., 31, (10, Supplement), S3-S13, doi:10.1016/j.csr.2010.02.008, 2011.

Droppo, I. G., Leppard, G. G., Liss, S. N., and Milligan, T. G.: Opportunities, needs, and strategic direction for research on flocculation in natural and engineered systems, in: Droppo, I. G., Leppard, G. G., Liss, S. N., and Milligan, T. G., (Eds.), Flocculation in Natural and Engineered Environmental Systems, CRC Press, London, 407−421, 2005.

Fischer, H.B., List, E.J., Koh, R.C.Y., Imberger, J., Brooks, N.H.: Mixing in Inland and Coastal Waters. Academic Press, Inc., 1979.

Harris, C. K. and Wiberg, P. L.: Approaches to quantifying long-term continental shelf sediment transport with an example from the northern California STRESS mid-shelf site, Cont. Shelf Res., 17, 1389−1418, 1997.

Harris, C. K. and Wiberg, P. L.: A two-dimensional, time-dependent model of suspended sediment transport and bed reworking for continental shelves, Comput. Geosci., 27, 6, 675−690, 2001.

Hill, P. S.: Sectional and discrete representations of floc breakage in agitated suspensions, Deep-Sea Res. PT I, 43, 5, 679−702, 1996.

Hirano, M.: River bed degradation with armouring, in: Proceedings, Japan Society of Civil Engineers, Vol. 195, Japan, 1971.

HydroQual, Inc.: A Primer for ECOMSED Version 1.4 Users Manual, HydroQual, Inc., Mahwah, NJ, 2004.

Jacobs, W., Le Hir, P., Van Kesteren, W., and Cann, P.: Erosion threshold of sand - mud mixtures, Cont. Shelf Res., 31, 10 Supplement, S14–S25, doi:10.1016/j.csr.2010.05.012, 2011.

Khelifa, A. and Hill, P. S.: Models for effective density and settling velocity of flocs. J. Hydraul. Res., 44, 3, 390–401, 2006.

Kranenburg, C.: The fractal structure of cohesive sediment aggregates, Estuar. Coast. Shelf Sci., 39, 451–460, 1994.

Krone, R. B.: Flume studies of the transport of sediment in estuarial shoaling processes, Final Report, Hydraulic Engineering Laboratory and Sanitary Engineering Research Laboratory, Univ. of California, Berkeley, 1962.

Krone, R. B.: A study of rheologic properties of estuarial sediments, Technical Bulletin 7, Vicksburg, MS., U.S. Army Corps of Engineers Communication on Tidal Hydrodynamics, 1963.

Le Hir, P., Cayocca, F., and Waeles, B.: Dynamics of sand and mud mixtures: A multiprocess-based modelling strategy, Cont. Shelf Res., 3, 10 Supplement, S135–S149, 2011.

Letter, J. V.: Significance of probabilistic parameterization in cohesive sediment bed exchange, Ph.D. Thesis, Univ. of Florida, Gainesville, 2009.

Letter, J. V. and Mehta, A. J.: A heuristic examination of cohesive sediment bed exchange in turbulent flows, Coast. Eng., 58, 779–789, 2011.

McAnally, W. H.: Aggregation and Deposition of Estuarial Fine Sediment, Ph.D. Thesis, Univ. of Florida, 382 pp, 1999.

McAnally, W. H. and Mehta, A. J.: Collisional aggregation of fine estuarial sediment, in: McAnally, W. H. and Mehta, A. J. (Eds.), Coastal and Estuarine Fine Sediment Processes, Elsevier, 19-39, 2001.

McCave, I. N. and Swift, S. A.: A physical model for the deposition of fine-grained sediments in the deep sea, Bull. Geol. Soc. Am., 87, 541–546, 1976.

Mehta, A. J.: An Introduction to the Hydraulics of Fine Sediment Transport, World Scientific, 1039 pp, 2014.

Merkel, U. H. and Kopmann, R.: A continuous vertical grain sorting model for Telemac & Sisyphe, in: Munoz, R. M. (Ed) River Flow 2012, Taylor & Francis, London, 2012.

Mitchener, H. and Torfs, H.: Erosion of mud/sand mixtures, Coast. Eng., 29, 1-2, 1–25, 1996.

Moriarty, J.M., Harris, C.K., Fennel, K., Friedrichs, M.A.M., Xu, K,, and Rabouille, C.: The roles of resuspension, diffusion and biogeochemical processes on oxygen dynamics offshore of the Rhône River, France: a numerical modeling study. Biogeosciences 14, 1919-1946, 2017.

Panagiotopoulos, I., Voulgaris, G., and Collins, M. B.: The influence of clay on the threshold of movement in fine sandy beds, Coast. Eng., 32, 19–43, 1997.

Rinehimer, J. P., Harris, C. K., Sherwood, C. R., and Sanford, L. P.: Sediment consolidation in a muddy, tidally-dominated environment: Model behavior and sensitivity, Estuarine and Coastal Modeling, Proceedings of the Tenth International Conference: 819−838, 2008.

Sanford, L. P.: Modeling a dynamically varying mixed sediment bed with erosion, deposition, bioturbation, consolidation, and armoring, Comput. Geosci., 34(10), 1263−1283, 2008.

Sherwood, C. R., Drake, D. E., Wiberg, P. L., and Wheatcroft, R. A.: Prediction of the fate of p,p'-DDE in sediment on the Palos Verdes shelf, California, USA, Cont. Shelf Res., 22, 6-7, 1025−1058, 2002.

Stone, M., Krishnappan, B. G., and Emelko, M. B.; The effect of bed age and shear stress on the particle morphology of eroded cohesive river sediment in an annular flume, Water Res., 42, 15, 4179−4187, doi: 10.1016/j.watres.2008.06.019, 2008.

Tambo, N. and Watanabe, Y.; Physical characteristics of flocs. I The floc density function and aluminium floc. Water Research 13, 409–419, 1979.

Umlauf, L. and Burchard, H.: A generic length-scale equation for geophysical turbulence models, J. Mar. Res., 61, 2, 235−265, 2002.

Verney, R., Lafite, R., Brun-Cottan, J. C., and Le Hir, P.: Behaviour of a floc population during a tidal cycle: Laboratory experiments and numerical modeling, Cont. Shelf Res., 31, S64−S83, doi:10.1016/j.csr.2010.02.005, 2011.

Warner, J. C., Sherwood, C. R., Arango, H. G., and Signell, R. P.: Performance of four turbulence closure models implemented using a generic length scale method, Ocean Model., 8, 1/2, 81−113, doi:10.1029/2004JC002691, 2005.

Warner, J. C., Sherwood, C. R., Signell, R. P., Harris, C. K., and Arango, H. G.: Development of a three-dimensional, regional, coupled wave, current, and sediment-transport model, Comput. Geosci., 34, 1284−1306, 2008.

Whitehouse, R. J. S., Soulsby, R. L., Roberts, W., and Mitchener, H.: Dynamics of Marine Muds, Thomas Telford, London, 2000.

Winterwerp, J. C.: On the Dynamics of High-Concentrated Mud Suspensions, Technical University of Delft, Delft, The Netherlands, 1999.

Winterwerp, J. C.: On the flocculation and settling velocity of estuarine mud, Cont. Shelf Res., 22, 9, 1339−1360, 2002.

Winterwerp, J. C. and Kranenburg, C. (Eds.): Fine Sediment Dynamics in the Marine Environment, Proceedings in Marine Science, Vol 5, Elsevier, Amsterdam, 2002.

Winterwerp, J. C., Maa, J. P.-Y., Sanford, L. P., and Schoellhamer, D. H.: On the sedimentation rate of cohesive sediment, in: Proceedings in Marine Science, 8, Elsevier, 209−226, 2007

Winterwerp, J. C. and van Kesteren, W. G. M.: Introduction to the Physics of Cohesive Sediment in the Marine Environment, Elsevier, Amsterdam, 2004.

Tables

Table S1. List of symbols

Symbol	Description	Typical or Default Value Used Here	Units
A	Probability function for two-particle collision among floc classes i and j		–
B	Fragmentation rate		1/s
C_v	Volume concentration		m^3 / m^3
C	Mass concentration		kg / m^3
D	Sediment (non-cohesive or cohesive) diameter	4e-6 – 2e-3	m
D_b	Sediment (bio)diffusivity		m^2 / s
D_{bs}	Sediment (bio)diffusivity at sediment-water interface		m^2 / s
D_{bm}	Sediment (bio)diffusivity at bottom of exponential profile		m^2 / s
D_f	Floc diameter	4e-6 – 2e-3	m
D_p	Primary particle diameter	4e-6 – 20e-6	m
E	Erosion rate		$kg\ m^{-2}\ s^{-1}$
E_0	Erosion rate parameter	~0.005 – 0.05	$kg\ m^{-2}\ s^{-1}$
$FDBC$	Floc distribution function due to collision breakup		–
$FDBS$	Floc distribution function due to shear breakup		–
F_p	Relative depth of interparticle (floc) penetration	0.1	–
F_y	Floc yield strength	10^{-10}	N
G	Turbulence shear rate	~0 - 20	1/s
G_a	Gain rate in floc class by aggregation		$m^{-3}s^{-1}$
G_{bc}	Gain rate in floc class by collision		$m^{-3}s^{-1}$

	breakup		
G_{bs}	Gain rate in floc class by shear breakup		$m^{-3}s^{-1}$
L_a	Loss rate from floc class by aggregation		$m^{-3}s^{-1}$
L_{bc}	Loss rate from floc class by collision breakup		$m^{-3}s^{-1}$
L_{bs}	Loss rate from floc class by shear breakup		$m^{-3}s^{-1}$
M	Erosion rate parameter	~0.005 – 0.05	$kg\ m^{-2}\ s^{-1}$ $Pa^{-1}\ m^{-2}$
N	Number concentration of floc particles		m^{-3}
NBED	Number of bed layers	1 to unlimited	–
NCS	Number of cohesive sediment classes	0 to unlimited	–
NNS	Number of non-cohesive sediment classes	0 to unlimited	–
NSED	Total number of sediment classes (NCS+NNS)	at least 1	–
P_c	Cohesive behavior parameter	0 to 1	–
T_c	Time scale for consolidation	~ 0 – 360,000	s
T_s	Time scale for swelling	$100 \times T_c$	s
a	dummy coefficient in (3 and S 24)	1	$Pa\ kg^{-1}\ m^{-2}$
a'	dimensional coefficient in (S 26)	~1 – 5	$m\ s^2$
b	non-dimensional coefficient	~0.3 – 0.6	–
c	Nudging coefficient	0 – 1	–
c_μ^0	Stability coefficient in turbulence model	varies depending on turbulence model	Table 2. in Warner et al. (2005)
f	Volume fraction of sediment class	0 – 1	–
f_c	Mass fraction of cohesive material in bed	0 – 1	–

f_{ceq}	Equilibrium fractional distribution of cohesive sediment	0 – 1	–
$f_{c\ thresh}$	Mass fraction threshold for fully cohesive behavior	0.2	–
$f_{nc\ thresh}$	Mass fraction threshold for fully non-cohesive behavior	0.03 – 0.1	–
g	Gravitational acceleration	9.81	m/s^2
gls	Second (length-scale) parameter in GLS turbulence model	varies depending on turbulence model	Table 1. in Warner et al. (2005)
gls_m	Coefficient in GLS turbulence model	"	"
gls_n	Coefficient in GLS turbulence model	"	"
gls_p	Coefficient in GLS turbulence model	"	"
h	Water depth	5 - 20	m
i	Index	1 to NBED, 1 to NCS	–
j	Index	1 to NBED, 1 to NCS	–
k	Index	1 to NBED, 1 to NCS	–
k_1	Coefficient in active-layer formula	0.007	m / Pa
k_2	Coefficient in active-layer formula	6	–
m	Floc mass		kg
m_{ec}	Cumulative mass eroded in erosion chamber		kg
m_{eq}	Equilibrium sediment mass		kg
m_{tot}	Total mass of sediment		kg
n_f	Fractal dimension	1.9 – 2.2	–
$offset$	Coefficient in equilibrium critical shear stress for erosion profile		ln(kg/m^2)
r	Denominator in biodiffusivity profile equation		m
s	Sea-surface elevation		m
$slope$	Coefficient in equilibrium critical		ln(kg/m^2)

	shear stress for erosion profile		
t	Time		s
t_{eq}	Equilibrium time scale		s
Δt	Model time step	1 – 100	s
tke	Turbulence kinetic energy		m^2/s^2
u	Water velocity	0 – 2	m/s
u_*	Shear velocity	0 – 0.05	m/s
w_s	Settling velocity	$10^{-5} – 10^{-3}$	m/s
x	Distance		m
z	Depth in sediment bed; Elevation above seafloor	0 – 2; 0 - 20	m
z_m	Depth in sediment to bottom of exponential biodiffusive mixing	0.005 – 0.10	m
z_s	Depth in sediment to bottom of exponential biodiffusive mixing	0.01 – 0.5	m
z_{zero}	Depth in sediment to bottom of biodiffusive mixing	0.02 - 2	m
z_0	Bottom roughness length	$10^{-5} – 10^{-2}$	m
z_ρ	Mass depth in sediment bed		kg/m^2
Δz	Bed-layer thickness	10^{-3} to 10^0	m
Δz_a	Active-layer thickness	10^{-4} to 10^{-2}	m
$\Delta z_{nl\ max}$	Maximum layer thickness	10^{-4} to 10^{-2}	m
α	Collision efficiency	0.35	–
β	Fragmentation rate coefficient	0.15	–
ε	Turbulence dissipation rate		m^2/s^3
κ	von Kármán's constant	0.41	–
μ	Dynamic viscosity	0.001	Pa s
ξ	Exponent coefficient	0.5	–
ρ_s	Particle density of sediment	2650	kg / m^3

ρ_f	Floc density	1200 - 2650	kg / m^3
ρ_w	Water density	1030	kg / m^3
τ_b	Bottom shear stress		Pa
τ_c	Critical shear stress for erosion		Pa
τ_{cb}	Bulk critical shear stress for erosion of cohesive bed		Pa
$\tau_{cb\,eq}$	Equilibrium bulk critical shear stress for erosion		Pa
$\tau_{cb\,min}$	Equilibrium bulk critical shear stress for erosion		Pa
$\tau_{cb\,max}$	Equilibrium bulk critical shear stress for erosion		Pa
τ_{ce}	Effective critical shear stress for erosion of mixed sediment		Pa
τ^{coll}	Floc collision induced shear stress		Pa
τ_d	Critical shear stress for deposition		Pa
τ_{dp}	Critical shear stress for deposition of the primary particles	0.03	Pa
τ_{ec}	Erosion chamber shear stress		Pa
τ_{sf}	Skin-friction component of bottom shear stress		Pa
τ^y	Floc strength		Pa
ν	Kinematic viscosity	10^{-6}	m^2/s

Table S2. Variables associated with the floc model FLOCMOD as implemented in ROMS/CSTMS, listed in order of appearance in the sediment.in input file.

Symbol in Text	Model Variable Name in FLOCMOD	Description	Typical or Default Value	Units
	l_ADS	Enable differential settling	F	True/False
	l_ASH	Enable shear aggregation	T	True/False
D_p	f_dp0	Primary particle size	4e-6	m
	f_dmax	Maximum particle size	Not used	m
	f_nb_frag	Number of fragments by shear erosion	2	-
α	f_alpha	Flocculation efficiency (range: 0 – 1)	0.35	-
β	f_beta	Shear fragmentation rate (0 – 1)	0.15	-
	f_ater	Ternary breakup: 0.5; Binary: 0.0	0.0	-
	f_ero_frac	Fraction of shear fragmentation term transferred to shear erosion (0 – 1)	0.0	-
	f_ero_nbfrag	Number of fragments induced by shear erosion	2.0	-
	f_ero_iv	Fragment size class	1	-
	f_collfragparam	Fragmentation rate for collision-induced breakup	0.01	-
	f_clim	Min. concentration below which floc processes are not calculated	0.001	kg / m^3
	l_testcase	Set G values to Verney et al. (2011) values	F	True/False
	MUD_FRAC_EQ	Fractional size class distribution for cohesive sediment in bed		NNS values; sum must be unity.
	t_dfloc	Time scale for floc evolution in the bed	200.0	s

Table S3. Sediment property parameters stored for each sediment class in ROMS. These are defined by the user in an input file with the generic name `sediment.in`.

Symbol	Array Name[a]	Description	Typical Range of Values	Units
D	SD50	Median sediment grain diameter	10^{-4} - 10	mm
m	CSED	Sediment concentration	0 - 20	kg / m^3
ρ	SRHO	Sediment grain density	2650	kg / m^3
w	WSED	Particle settling velocity	10^{-2} - 100	mm / s
E_0	ERATE	Erosion rate coefficient	$10^{-3} - 10^{-2}$	kg m^{-2} s^{-1}
τ_{ce}	TAU_CE	Critical shear stress for erosion	0.02 - 5	Pa = N / m^2
τ_d	TAU_CD	Critical shear stress for erosion	Not well constrained	Pa = N / m^2
ϕ	POROS	Porosity	0.1 – 0.9	m^3 / m^3

[a]Array names are preceded by either SAND_ or MUD_ for non-cohesive and cohesive sediment, respectively.

Table S4. Seabed properties stored at each horizontal grid cell in the BOTTOM array in ROMS/COAWST.

Symbol (this paper)	Array Index Name (in model)	Description	Typical or Default Value for parameters introduced in this paper	Units
D_r	isd50	Representative grain diameter[a]		m
$\langle \rho_s \rangle$	idens	Representative sediment density[a]		kg / m^3
$\langle w_s \rangle$	iwsed	Representative particle settling velocity[a]		kg / m^3
$\langle \tau_{ce} \rangle$	itauc	Representative critical shear stress for erosion (kinematic units)		m^2 / s^2
	irlen	Ripple wavelength		m
	irhgt	Ripple height		m
	ibwave	Near-bottom wave-orbital excursion amplitude		m
	izdef	Default bottom roughness		m
	izapp	Apparent bottom roughness		m
	izNik	Nikuradse bottom roughness		m
	izbio	Biological bottom roughness		m
	izbfm	Bedform bottom roughness		m
	izbld	Saltation bottom roughness		m
	izwbl	Bottom roughness used in wave model		m
z_a	iactv	Active-layer thickness		m
	ishgt	Saltation height		m
	idefx	Erosion flux		kg m^{-2} s^{-1}

idnet	Net erosion or deposition		kg m-2
idoff	Offset for erodibility profile[b]	[-0.469, 0.3]	
idslp	Slope of erodibility profile[b]	[1.7, 2]	
idtim	Equilibrium time scale for erodibility profile[b]	[2, 8, 24] hours	s
idbmx	Bed biodiffusivity maximum[c]	$[10^{-10}, 10^{-5}]$	m^2 / s
idbmm	Bed biodiffusivity minimum[c]	$[10^{-12}, 10^{-8}]$	m^2 / s
idbzs	Depth to bottom of uniform biodiffusivity profile[c]	0.002	m
idbzm	Depth to bottom of linear biodiffusivity profile[c]	0.08	m
idbzp	Depth to bottom of non-zero biodiffusivity profile[c]	0.01	m
idprp	Cohesive behavior[d]	0-1	-

[a]Calculated as a fraction-weighted geometric mean.

[b]Only required for cohesive or mixed sediment calculations.

[c]Only required for bed mixing.

[d]Only required for mixed sediment calculations.

Figures

```
if SEDIMENT
  sediment.F - Initiate sediment routines
  if BEDLOAD
    sed_bedload.F - Bedload transport
  endif
  if SUSPLOAD
    if SED_FLOCS
      sed_flocs.F - Floc dynamics
    endif
    sed_settling.F - Suspended sediment settling
    sed_fluxes.F - Erosion / Deposition
  endif
  if COHESIVE_BED or MIXED_BED
    sed_bed_cohesive.F *- Cohesive / mixed stratigraphy
    if SED_FLOCS and SED_DEFLOC
      sed_bed_cohesive.F *- Adjust floc distribution in bed
    endif
  elseif NONCOHESIVE_BED2
    sed_bed2.F *- Non-cohesive stratigraphy (revised)
  else
    sed_bed.F - Non-cohesive stratigraphy (original)
  endif
  if SED_BIODIFF
    sed_biodiff.F* - Biodiffusive mixing of bed
  endif
  sed_surface.F - Update surface properties
```

Figure S 1. Pseudocode describing components of the CSTMS sediment module activated by C preprocessor keywords (**BOLD**) during compilation. Filenames in the source code are indicated with `courier font`. Components with asterisks (*) are new.
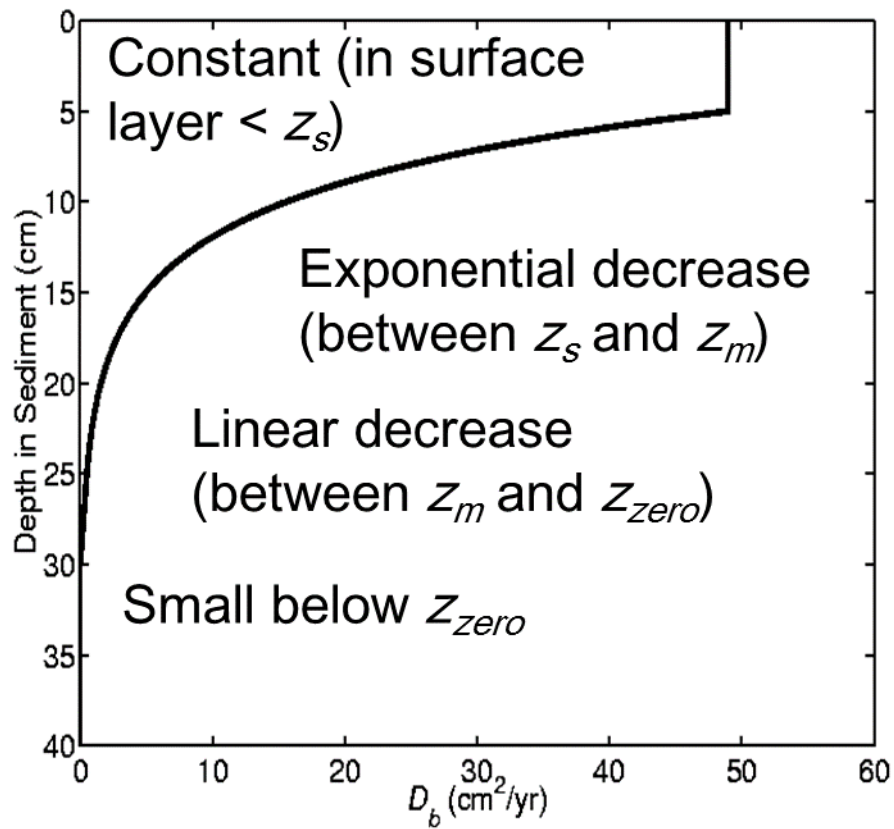
Figure S 2. Biodiffusivity profile defined by five user-specified parameters. In this example, $D_{bs} = 48$ cm^2/yr.